# Dirichlet-to-Neumann Map Method for Analyzing Hole Arrays in a Slab

Lijun Yuan and Ya Yan Lu

*Department of Mathematics, City University of Hong Kong*
*Kowloon, Hong Kong*

A rigorous and efficient computational method is developed to calculate transmission and reflection spectra for finite number of air-hole arrays in a slab, where the incident waves are propagating modes of the slab. The method is a three-dimensional extension of the Dirichlet-to-Neumann (DtN) map method previously developed for ideal two-dimensional photonic crystals which are infinite and invariant in one spatial direction. The method relies on the DtN maps of the unit cells to avoid repeated calculations in identical unit cells. The DtN map of a unit cell is constructed using eigenmode expansions in the vertical direction (perpendicular to the slab) and cylindrical wave expansions in the horizontal directions.

## 1. Introduction

In the last two decades, photonic crystals (PhCs) [1] have been extensively explored for their unusual abilities to control and manipulate light. The most important property of a PhC is the existence of bandgaps, i.e., frequency intervals in which propagating waves do not exist. Based on the bandgap effect, microcavities, waveguides and more complicated structures can be developed in a PhC by introducing defects, and these PhC devices may have significant applications in future photonic integrated circuits. In principle, full light confinement by the bandgap effect can only occur in a three-dimensional (3D) PhC which has three linearly independent periodic directions. Since the fabrication of a 3D PhC under the sub-micrometer scale is a very challenging and expensive task, much attention has been turned to photonic crystal slabs which are 3D structures with a two-dimensional (2D) periodicity. Typically, a PhC slab is obtained by etching a triangular lattice of air-holes in a layered medium, such as a dielectric slab of high refractive index surrounded by lower-index materials. PhC slabs can confine light via the bandgap effect in the plane of periodicity (parallel to the slab), but they cannot prevent out-of-plane radiation loss, since the vertical confinement by index guiding is imperfect. Nevertheless, since PhC slabs are relatively easy to fabricate with existing technologies, they have been used to design many interest photonic devices.

To analyze basic properties of a PhC slab and to design photonic components and devices in a PhC slab, efficient numerical methods are needed. The mathematical problems can be classified as eigenvalue problems for band structures, waveguide modes and cavity modes, and boundary value problems for general components and devices, such as waveguide bends, branches, couplers, filters, interferometers, etc. Since a PhC slab is a 3D structure, these mathematical problems are computationally expensive. This is especially true for boundary value problems involving many unit cells. One of the most important boundary value problem is to compute the transmission and reflection spectra for finite number of hole arrays in a slab. These spectra are useful, since in practice, waveguides or other components, are separated only by a finite number of unit cells. They are also closely related to experimental setups for verifying the bandgaps of the PhC slab.

One way to reduce the computation difficulties of these boundary value problems is to use a 2D model as in the effective index method [2], or simplify the problem by keeping only the propagating Bloch modes of the PhC slab [3]. However, it has been recognized that the 2D models are not always accurate. One reason is that the 2D models cannot accurately account for the out-of-plane radiation loss in PhC slabs. The finite-difference time-domain (FDTD) method [4] is a widely used rigorous method to simulate lightwaves in photonic structures, but it is also prohibitively expensive, since small grid sizes are needed to resolve interfaces with large index-contrast, small time steps are needed to ensure numerical stability, and the computational domain may be very large compared with the wavelength. On the other hand, standard frequency domain methods, such as the finite element method [5, 6], give rise to very large, sparse, indefinite and complex linear systems that are difficult to solve by existing numerical linear algebra techniques. However, special frequency-domain methods can be developed to take advantage of the available geometric features. The multipole method [7–10] is a classical semi-analytic method for analyzing scattering problems associated with cylinders and spheres. It has been extended to PhC slabs based on eigenmode expansions in the vertical direction [11], where the slab is assumed to be horizontal. While the multipole method is quite suitable for a slab with a finite number of holes, it becomes rather complicated when the slab contains infinite number of holes due to the need to evaluate lattice sums. The integral equation method [12] is another approach that can make use of the special geometry. For PhC slabs, an integral equation method with an accelerated iterative solver was presented in [13].

Recently, some efficient numerical methods based on the Dirichlet-to-Neumann (DtN) maps of the unit cells have been developed to analyze ideal 2D PhCs which are infinite and invariant in one direction [14,15]. The DtN map of a unit cell is an operator (approximated by a small matrix) that provides the relation between the wave field and its normal derivative on the cell boundary, and it can be used to avoid repeated calculations in identical unit

cells. For computing transmission and reflection spectra, the DtN maps are used together with an operator marching scheme that reduces memory requirement [15–19]. For simulating general PhC devices, the DtN map method also provides a rigorous boundary condition for terminating semi-infinite PhC waveguides [20, 21]. In this paper, we extend the DtN map method to PhC slabs for computing transmission and reflection spectra. In the vertical direction, we use eigenmode expansions as in [11]. The main advantages of the DtN map method for ideal 2D problems are preserved. In particular, our method avoids lattice sums, and it appears to be much simpler than the multipole method [11].

The rest of the paper is organized as follows. The mathematical problem including proper boundary conditions is formulated in Section 2. For solving the boundary value problems associated with transmission and reflection spectra, the operator marching scheme is presented in Section 3. Various operators used in the operator marching scheme are represented by matrices based on vertical mode expansions in Section 4. The DtN map of a unit cell is constructed in Section 5, using general solutions in the unit cell given in vertical mode and horizontal cylindrical wave expansions. In Section 6, we briefly discuss a fourth order finite difference scheme for discretizing the vertical direction and solving the vertical modes. To validate our method, we present a few numerical examples in Section 7.

## 2. Problem formulation

We consider an infinite slab parallel to the $xy$ plane and surrounded by a homogeneous medium with a lower refractive index, such as air. On the slab, there are one or more arrays of circular cylindrical holes, where each array consists of infinite number of holes arranged periodically in the $x$ direction with period $L$. The centers of the holes are located on a triangular lattice with lattice constant $L$. A particular case with five hole arrays is shown in Fig. 1. The hole arrays are assumed to be bounded by two planes at $y = 0$ and $y = D$. For

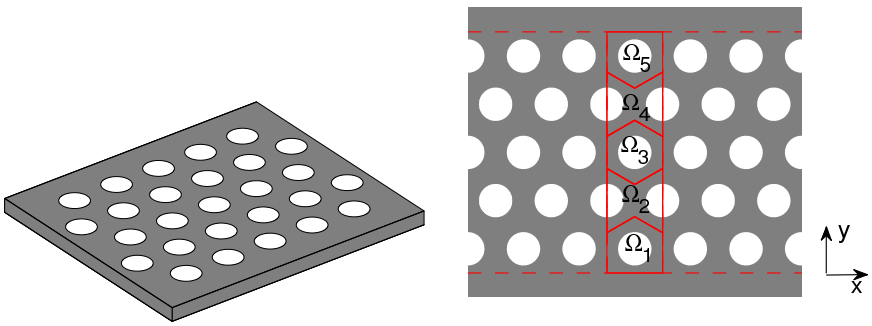


Fig. 1. A dielectric slab with five arrays of holes on a triangular lattice. Left: three-dimensional view; Right: top view.

$y < 0$ and $y > D$, the structure is the original slab without holes.

Our starting point is the Maxwell's equations. Assuming a time dependence $\exp(-i\omega t)$, where $\omega$ is the angular frequency, the electromagnetic field satisfies the following frequency-domain Maxwell's equations:

$$\nabla \times \mathbf{E} = ik_0\mu\mathbf{H}, \quad \nabla \times \mathbf{H} = -ik_0\varepsilon\mathbf{E}, \tag{1}$$

where $\mathbf{H}$ is the magnetic field scaled by the free space impedance, $k_0 = \omega/c$ is the free space wavenumber, $c$ is the speed of light in vacuum, $\varepsilon$ is the dielectric constant (or relative permittivity) and $\mu$ is the relative magnetic permeability ($\mu = 1$ for nonmagnetic media). For a general 3D structure, $\varepsilon$ and $\mu$ are functions of $x$, $y$ and $z$.

Away from the holes, the structure has only a one-dimensional (1D) profile, that is, $\varepsilon$ and $\mu$ depend only on $z$. In that case, the electromagnetic field can be decomposed as transverse electric (TE) and transverse magnetic (TM) waves, such that the $z$ components of the electric and magnetic fields are zero, respectively. Meanwhile, the slab without the holes works as a waveguide, and it may support a few TE and TM guided modes. The TE modes satisfy the eigenvalue problem

$$\mu\frac{d}{dz}\left(\frac{1}{\mu}\frac{d\phi^{(1)}}{dz}\right) + k_0^2\varepsilon\mu\phi^{(1)} = [\eta^{(1)}]^2\phi^{(1)}, \quad -\infty < z < \infty, \tag{2}$$

where $\eta^{(1)}$ is the propagation constant, $\phi^{(1)} = \phi^{(1)}(z)$ is the profile of the $x$ and $y$ components of the electric field, and the $z$ component of the magnetic field is proportional to $\mu^{-1}\phi^{(1)}$. Similarly, the TM modes give rise to the eigenvalue problem

$$\varepsilon\frac{d}{dz}\left(\frac{1}{\varepsilon}\frac{d\phi^{(2)}}{dz}\right) + k_0^2\varepsilon\mu\phi^{(2)} = [\eta^{(2)}]^2\phi^{(2)}, \quad -\infty < z < \infty, \tag{3}$$

where $\eta^{(2)}$ is the propagation constant, $\phi^{(2)} = \phi^{(2)}(z)$ is the profile of the $x$ and $y$ components of the magnetic field, and the $z$ component of the electric field is proportional to $\varepsilon^{-1}\phi^{(2)}$. The guided modes must satisfy the boundary condition

$$\phi^{(p)}(z) \to 0 \quad \text{as} \quad |z| \to \infty, \quad \text{for} \quad p = 1, 2. \tag{4}$$

The slab waveguide has only a finite number of guided modes and they are denoted by $\eta_j^{(p)}$ and $\phi_j^{(p)}$ ($p = 1$ and 2) for a few positive integers $j$ starting from $j = 1$. In particular, $\eta_1^{(p)}$ and $\phi_1^{(p)}$, i.e. $j = 1$, are used to denote the fundamental TE or TM mode which has the largest propagation constant (for each $p$).

For the slab with hole arrays, we specify an incident wave for $y > D$. The incident wave is typically the fundamental TE or TM mode propagating towards the hole arrays. If the TE mode is used, the incident wave is

$$H_z^{(i)} = \frac{1}{\mu(z)}\phi_1^{(1)}(z)\exp[i(\alpha_0 x - \beta_{1,0}^{(1)} y)], \quad E_z^{(i)} = 0, \tag{5}$$

where $\alpha_0$ and $\beta_{1,0}^{(1)}$ satisfy $\alpha_0^2 + [\beta_{1,0}^{(1)}]^2 = [\eta_1^{(1)}]^2$ and $\beta_{1,0}^{(1)}$ is positive. The first and second subscripts in $\beta_{1,0}^{(1)}$ represent the first vertical mode and zeroth diffraction order, respectively. If the incident angle (with respect to the $y$ axis) is $\theta_{1,0}^{(1)}$, then $\alpha_0 = \eta_1^{(1)} \sin(\theta_{1,0}^{(1)})$ and $\beta_{1,0}^{(1)} = \eta_1^{(1)} \cos(\theta_{1,0}^{(1)})$. If the TM mode is used, the incident wave is

$$E_z^{(i)} = \frac{1}{\varepsilon(z)} \phi_1^{(2)}(z) \exp[i(\alpha_0 x - \beta_{1,0}^{(2)} y)], \quad H_z^{(i)} = 0, \tag{6}$$

where $\alpha_0$ and $\beta_{1,0}^{(2)}$ satisfy $\alpha_0^2 + [\beta_{1,0}^{(2)}]^2 = [\eta_1^{(2)}]^2$ and $\beta_{1,0}^{(2)} > 0$. The angle of incidence $\theta_{1,0}^{(2)}$ can be similarly defined. Notice that we have used the same $\alpha_0$ for both cases. Meanwhile, only the $z$ components of the incident wave are specified. The other four components can be determined from the two $z$ components and they are not needed in our computation.

The incident wave gives rise to a reflected wave for $y > D$ and a transmitted wave for $y < 0$. Although the incident wave is only a single TE or TM mode propagating with a fixed incident angle as a plane wave in the horizontal plane, the reflected and transmitted waves must include both TE and TM waves, all vertical modes and all diffraction orders. The $k$-th diffraction order associated with $j$-th TE or TM mode behaves like a plane wave with wave vector $(\alpha_k, \beta_{jk}^{(p)})$ in the $xy$ plane, where

$$\alpha_k = \alpha_0 + 2\pi k/L, \quad \beta_{jk}^{(p)} = \sqrt{[\eta_j^{(p)}]^2 - \alpha_k^2}, \quad p = 1, 2. \tag{7}$$

In the above, the imaginary part of $\beta_{jk}^{(p)}$ is required to be non-negative. Therefore, the $z$ components of the reflected and transmitted waves can be written as

$$H_z^{(r)} = \frac{1}{\mu(z)} \sum_j \sum_{k=-\infty}^{\infty} R_{jk}^{(1)} \, \phi_j^{(1)}(z) \exp[i(\alpha_k x + \beta_{jk}^{(1)} y)], \tag{8}$$

$$E_z^{(r)} = \frac{1}{\varepsilon(z)} \sum_j \sum_{k=-\infty}^{\infty} R_{jk}^{(2)} \, \phi_j^{(2)}(z) \exp[i(\alpha_k x + \beta_{jk}^{(2)} y)], \tag{9}$$

$$H_z^{(t)} = \frac{1}{\mu(z)} \sum_j \sum_{k=-\infty}^{\infty} T_{jk}^{(1)} \, \phi_j^{(1)}(z) \exp[i(\alpha_k x - \beta_{jk}^{(1)} y)], \tag{10}$$

$$E_z^{(t)} = \frac{1}{\varepsilon(z)} \sum_j \sum_{k=-\infty}^{\infty} T_{jk}^{(2)} \, \phi_j^{(2)}(z) \exp[i(\alpha_k x - \beta_{jk}^{(2)} y)], \tag{11}$$

where $R_{jk}^{(p)}$ and $T_{jk}^{(p)}$ ($p = 1, 2$) are the reflection and transmission amplitudes to be determined. Since the slab waveguide has only a finite number of guided modes, the sums over $j$ above appear to be finite sums. However, the incident wave also excites the radiation and evanescent modes. Therefore, strictly speaking, we should replace each sum over $j$ above by a finite sum for the guided modes and an integral over the continuous spectrum for radiation and evanescent modes [22]. Since the explicit integral representation of the continuous

spectrum is complicated, we adopt a more practical approach. In our actual numerical implementation, the $z$ axis will be truncated by perfectly matched layers (PMLs) [23,24], then the continuous spectrum is approximated by a discrete sequence of eigenvalues. With this approximation, the index $j$ in (8)-(11) goes through all positive integers, i.e., $j = 1, 2, ..., \infty$. Further details are given in Section 4.

If $\phi_j^{(1)}$ is a guided vertical TE mode, the $k$-th transmitted diffraction order associated with $\phi_j^{(1)}$ is the field with its $H_z$ component given by the $(j,k)$-th term in the right hand side of Eq. (10), i.e., $\mu^{-1}T_{jk}^{(1)}\phi_j^{(1)}(z)\exp[i(\alpha_k - \beta_{jk}^{(1)}y)]$. When $\varepsilon$ and $\mu$ are both real and if $\beta_{jk}$ is real (and positive), it is a propagating diffraction order which carries a power given by

$$\mathrm{TP}_{jk}^{(1)} = |T_{jk}^{(1)}|^2 \frac{\beta_{jk}^{(1)}}{[\eta_j^{(1)}]^2} \int_{-\infty}^{\infty} \frac{1}{\mu(z)} |\phi_j^{(1)}(z)|^2 dz. \tag{12}$$

Similarly, the power carried by the $k$-th propagating transmitted order associated with $j$-th TM vertical mode is

$$\mathrm{TP}_{jk}^{(2)} = |T_{jk}^{(2)}|^2 \frac{\beta_{jk}^{(2)}}{[\eta_j^{(2)}]^2} \int_{-\infty}^{\infty} \frac{1}{\varepsilon(z)} |\phi_j^{(2)}(z)|^2 dz. \tag{13}$$

The total transmitted power (TP) is given by

$$\mathrm{TP} = \sum_{j,k} \left[ \mathrm{TP}_{jk}^{(1)} + \mathrm{TP}_{jk}^{(2)} \right], \tag{14}$$

where $j$ goes through only the guided modes and $k$ goes through only the propagating diffraction orders associated with each guided mode. The incident power (IP) and total reflected power (RP) are similarly defined. Notice that the incident wave given in (5) or (6) corresponds to the zeroth diffraction order associated with the first TE or TM vertical mode and the coefficient is 1. We define the transmittance (or relative transmitted power) as the ratio of TP and IP, reflectance (or relative transmitted power) as the ratio of RP and IP, and the out-of-plane radiation loss as $1 - (\mathrm{TP} + \mathrm{RP})/\mathrm{IP}$.

For a given incident wave, we can formulate the mathematical problem on the domain

$$\Omega = \{(x, y, z) \ : \ 0 < x < L,\, 0 < y < D,\, -\infty < z < \infty\}. \tag{15}$$

Notice that $\Omega$ covers one period in the $x$ direction, the interval $(0, D)$ in the $y$ direction, and it is still unbounded in $z$. The formulation in $\Omega$ requires proper boundary conditions. The boundary condition for $|z| \to \infty$ is the standard outgoing radiation condition which will be approximated by PMLs in Section 4. Since the structure is periodic in $x$ and the incident wave depends on $x$ as $\exp(i\alpha_0 x)$, the electromagnetic field is quasi-periodic. Let $\mathbf{w} = [H_z, E_z]^T$ be the column vector of the two $z$ components, then the quasi-periodic condition is

$$\mathbf{w}(x + L, y, z) = \rho \mathbf{w}(x, y, z) \quad \text{for} \quad \rho = e^{i\alpha_0 L}. \tag{16}$$

This implies that

$$\mathbf{w}(L,y,z)=\rho\mathbf{w}(0,y,z),\quad \frac{\partial\mathbf{w}}{\partial x}(L,y,z)=\rho\frac{\partial\mathbf{w}}{\partial x}(0,y,z). \tag{17}$$

To write down the boundary conditions at $y=0$ and $y=D$, we need to define two linear operators $\mathcal{S}^{(p)}$ $(p=1,\,2)$ which will be approximated by matrices. These two operators act on functions of $x$ and $z$ which are also quasi-periodic functions of $x$. Let $f(x,z)$ be such a function, we first expand $\mu f$ in the vertical TE modes as

$$\mu(z)f(x,z)=\sum_{j=1}^{\infty}\tilde{f}_j(x)\phi_j^{(1)}(z).$$

Since $f$ is quasi-periodic in $x$, so are $\tilde{f}_j$, i.e., $\tilde{f}_j(x+L)=\rho\tilde{f}_j(x)$. Therefore, we can expand $\tilde{f}_j$ in its Fourier series and obtain

$$f(x,z)=\frac{1}{\mu(z)}\sum_{j=1}^{\infty}\sum_{k=-\infty}^{\infty}\hat{f}_{jk}\,\phi_j^{(1)}(z)\exp(i\alpha_k x),$$

where $\hat{f}_{jk}$ are the Fourier coefficients of $\tilde{f}_j$. The operator $\mathcal{S}^{(1)}$ is defined by its eigenfunctions $\mu^{-1}\phi_j^{(1)}(z)\exp(i\alpha_k x)$ and the corresponding eigenvalues $\beta_{jk}^{(1)}$, namely

$$\mathcal{S}^{(1)}\left[\frac{1}{\mu(z)}\phi_j^{(1)}(z)\exp(i\alpha_k x)\right]=\beta_{jk}^{(1)}\left[\frac{1}{\mu(z)}\phi_j^{(1)}(z)\exp(i\alpha_k x)\right],$$

for $1\le j<\infty$ and $-\infty<k<\infty$. Since $\mathcal{S}^{(1)}$ is supposed to be linear, we have

$$[\mathcal{S}^{(1)}f](x,z)=\frac{1}{\mu(z)}\sum_{j=1}^{\infty}\sum_{k=-\infty}^{\infty}\beta_{jk}^{(1)}\hat{f}_{jk}\,\phi_j^{(1)}(z)\exp(i\alpha_k x).$$

If we evaluate the $y$ derivatives of $H_z^{(r)}$ and $H_z^{(t)}$ by (8) and (10), it is easy to obtain

$$\frac{\partial H_z^{(r)}}{\partial y}=i\mathcal{S}^{(1)}H_z^{(r)},\quad \frac{\partial H_z^{(t)}}{\partial y}=-i\mathcal{S}^{(1)}H_z^{(t)}. \tag{18}$$

Similarly, we define the linear operator $\mathcal{S}^{(2)}$ by

$$\mathcal{S}^{(2)}\left[\frac{1}{\varepsilon(z)}\phi_j^{(2)}(z)\exp(i\alpha_k x)\right]=\beta_{jk}^{(2)}\left[\frac{1}{\varepsilon(z)}\phi_j^{(2)}(z)\exp(i\alpha_k x)\right]$$

for $j\ge 1$ and all $k$, then

$$\frac{\partial E_z^{(r)}}{\partial y}=i\mathcal{S}^{(2)}E_z^{(r)},\quad \frac{\partial E_z^{(t)}}{\partial y}=-i\mathcal{S}^{(2)}H_z^{(t)}. \tag{19}$$

Let $\mathcal{S}$ be the $2 \times 2$ matrix operator with the diagonals $\mathcal{S}^{(1)}$ and $\mathcal{S}^{(2)}$ and using $\mathbf{w}$ for the two $z$ components, then (18) and (19) can be combined as

$$\frac{\partial \mathbf{w}^{(r)}}{\partial y} = i\mathcal{S}\mathbf{w}^{(r)}, \quad \frac{\partial \mathbf{w}^{(t)}}{\partial y} = -i\mathcal{S}\mathbf{w}^{(t)}. \tag{20}$$

Since the incident wave is given for $y > D$ only, we have $\mathbf{w} = \mathbf{w}^{(t)}$ for $y < 0$, thus the boundary condition at $y = 0$ is

$$\frac{\partial \mathbf{w}}{\partial y} = -i\mathcal{S}\mathbf{w}, \quad y = 0. \tag{21}$$

Meanwhile, it is easy to verify that the incident wave satisfies

$$\frac{\partial \mathbf{w}^{(i)}}{\partial y} = -i\mathcal{S}\mathbf{w}^{(i)}.$$

Since $\mathbf{w} = \mathbf{w}^{(i)} + \mathbf{w}^{(r)}$ for $y > D$, we can eliminate $\mathbf{w}^{(r)}$ and obtain the boundary condition:

$$\frac{\partial \mathbf{w}}{\partial y} = i\mathcal{S}\mathbf{w} - 2i\mathcal{S}\mathbf{w}^{(i)}, \quad y = D. \tag{22}$$

In the above, we have implicitly assumed that $y = 0$ and $y = D$ are not material interfaces. If this is not true, then $\partial_y \mathbf{w}$ is not continuous and the boundary conditions (21) and (22) should be set at $y = 0^-$ and $y = D^+$, respectively.

## 3. Operator marching scheme

In this section, we present the operator marching scheme as a special method for solving the boundary value problem (1,17,21,22). The operator marching scheme is a technique similar to the scattering matrix and transmittance/admittance matrix methods described in [26–29]. It has its origin in a work on acoustic waveguides [30], and it has been applied to optical waveguide problems [31, 32] and PhC problems [15–19]. The main idea is to reduce the boundary value problem to an "initial value problem" for a pair of operators. This leads to reduced computer memory requirement and the possibility of developing efficient implementations utilizing special geometric features of the structure.

We start by dividing the domain $\Omega$ given in (15) into sub-domains $\Omega_1$, $\Omega_2$, ..., $\Omega_{l_*}$, where $l_*$ is the total number of sub-domains. For the slab with five hole-arrays shown in Fig. 1, the top view of the five sub-domains are shown in Fig. 1(right). These sub-domains are 3D cylindrical volumes with possible cross sections shown in Fig. 2. For simplicity, we call these sub-domains unit cells, including non-convex sub-domains and modified sub-domains near the boundaries at $y = 0$ and $y = D$. These unit cells are bounded by the two surfaces at $x = 0$ and $x = L$, and separated by surfaces $\Gamma_0$, $\Gamma_1$, ..., $\Gamma_{l_*}$, where $\Gamma_0$ and $\Gamma_{l_*}$ denote the two flat surfaces at $y = 0$ and $y = D$. Among the six different unit cells shown in Fig. 2,

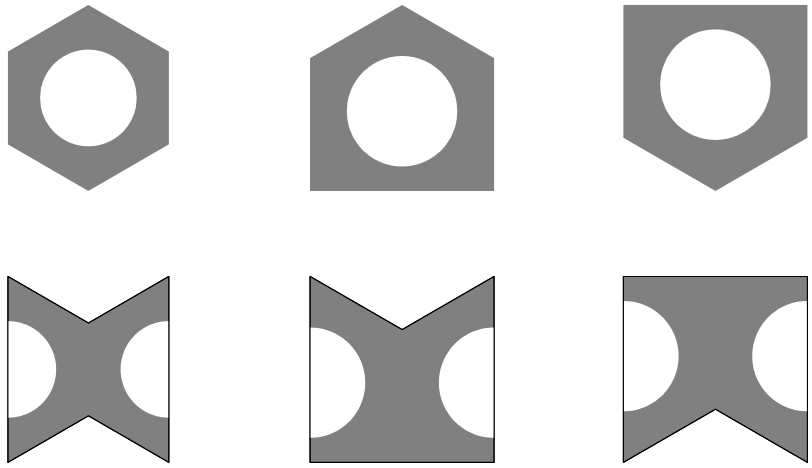

Fig. 2. Possible cross sections of the sub-domains $\Omega_l$ for a triangular lattice of air-holes on a slab.

we have three regular unit cells with convex cross sections that contain entire air-holes, and three shifted unit cells with non-convex cross sections that contain half air-holes.

On the surface $\Gamma_l$, we choose a unit normal vector $\nu$ with a positive $y$ component and define two operators $\mathcal{Q}_l$ and $\mathcal{Y}_l$ by

$$\mathcal{Q}_l \, \mathbf{w}_l = \partial_\nu \mathbf{w}_l, \quad \mathcal{Y}_l \, \mathbf{w}_l = \mathbf{w}_0, \tag{23}$$

where $\mathbf{w}$ is the vector for the two $z$ components of an arbitrary electromagnetic field satisfying the Maxwell's equations (1), the quasi-periodic condition (17) and the boundary condition (21) at $y = 0$, $\mathbf{w}_l$ and $\partial_\nu \mathbf{w}_l$ denote $\mathbf{w}$ and $\partial_\nu \mathbf{w}$ on $\Gamma_l$, respectively. Notice that boundary condition (22) at $y = D$ is not included in the above definition, thus the two equations in (23) are supposed to be valid for wave fields associated with any incident wave. The operator $\mathcal{Q}_l$ is a global DtN operator that links $\mathbf{w}$ to its normal derivative on $\Gamma_l$ for the global field satisfying (21) and (17). The operator $\mathcal{Y}_l$ is a fundamental solution operator that links $\mathbf{w}$ on $\Gamma_l$ to $\mathbf{w}$ on $\Gamma_0$. For the proper definition of $\mathcal{Q}_l$, we need to assume that $\Gamma_l$ does not coincide with a material interface, otherwise $\partial_\nu \mathbf{w}$ is not continuous and we must define $\mathcal{Q}_l$ based on one-sided limits. Matrix approximations of these operators will be discussed in Section 4.

On $\Gamma_0$ (i.e. $y = 0$), these two operators are known from boundary condition (21) and the definition of $\mathcal{Y}_0$, that is

$$\mathcal{Q}_0 = -i\mathcal{S}, \quad \mathcal{Y}_0 = \mathcal{I}, \tag{24}$$

where $\mathcal{I}$ is the identity operator. If we know $\mathcal{Q}_{l_*}$ and $\mathcal{Y}_{l_*}$ (defined on $\Gamma_{l_*}$, i.e., at $y = D$),

then boundary condition (22) gives us the following equation to solve the total field on $\Gamma_{l_*}$:

$$(\mathcal{Q}_{l_*} - i\mathcal{S})\mathbf{w}_{l_*} = -2i\mathcal{S}\mathbf{w}^{(i)}. \tag{25}$$

Furthermore, the total field on $\Gamma_0$ is given by

$$\mathbf{w}_0 = \mathcal{Y}_m \mathbf{w}_{l_*}. \tag{26}$$

The reflected wave can be obtained by subtracting $\mathbf{w}^{(i)}$ from $\mathbf{w}_{l_*}$. The transmitted wave at $y = 0$ is exactly $\mathbf{w}_0$.

Clearly, the key step is to calculate $\mathcal{Q}_l$ and $\mathcal{Y}_l$ from the given $\mathcal{Q}_{l-1}$ and $\mathcal{Y}_{l-1}$. This requires the so-called reduced DtN map $\mathcal{M}$ of the unit cell $\Omega_l$ satisfying

$$\mathcal{M}\begin{bmatrix}\mathbf{w}_l\\ \mathbf{w}_{l-1}\end{bmatrix} = \begin{bmatrix}\mathcal{M}_{11} & \mathcal{M}_{12}\\ \mathcal{M}_{21} & \mathcal{M}_{22}\end{bmatrix}\begin{bmatrix}\mathbf{w}_l\\ \mathbf{w}_{l-1}\end{bmatrix} = \begin{bmatrix}\partial_\nu \mathbf{w}_j\\ \partial_\nu \mathbf{w}_{j-1}\end{bmatrix}, \tag{27}$$

where $\mathbf{w}$ represents the electromagnetic field satisfying the Maxwell's equations (1) in $\Omega_l$ and the quasi-periodic condition (17). Notice that $\mathcal{M}$ is a $2\times 2$ matrix operator, where each block is an operator. From (23) and (27), we obtain the following marching formulas:

$$\mathcal{Z} = (\mathcal{Q}_{l-1} - \mathcal{M}_{22})^{-1}\mathcal{M}_{21}, \tag{28}$$

$$\mathcal{Q}_l = \mathcal{M}_{11} + \mathcal{M}_{12}\mathcal{Z}, \tag{29}$$

$$\mathcal{Y}_l = \mathcal{Y}_{l-1}\mathcal{Z}. \tag{30}$$

The reduced DtN maps are related to the (unreduced) DtN maps of the unit cells. If $\Omega_l$ is a regular unit cell, its DtN map is the $4\times 4$ matrix operator $\Lambda$ satisfying

$$\Lambda\begin{bmatrix}\mathbf{w}_l\\ \mathbf{w}_{l-1}\\ \mathbf{w}|_{x=L}\\ \mathbf{w}|_{x=0}\end{bmatrix} = \begin{bmatrix}\Lambda_{11} & \Lambda_{12} & \Lambda_{13} & \Lambda_{14}\\ \Lambda_{21} & \Lambda_{22} & \Lambda_{23} & \Lambda_{24}\\ \Lambda_{31} & \Lambda_{32} & \Lambda_{33} & \Lambda_{34}\\ \Lambda_{41} & \Lambda_{42} & \Lambda_{43} & \Lambda_{44}\end{bmatrix}\begin{bmatrix}\mathbf{w}_l\\ \mathbf{w}_{l-1}\\ \mathbf{w}|_{x=L}\\ \mathbf{w}|_{x=0}\end{bmatrix} = \begin{bmatrix}\partial_\nu \mathbf{w}_l\\ \partial_\nu \mathbf{w}_{l-1}\\ \partial_x \mathbf{w}|_{x=L}\\ \partial_x \mathbf{w}|_{x=0}\end{bmatrix}, \tag{31}$$

where $\mathbf{w}$ corresponds to an arbitrary electromagnetic field satisfying the Maxwell's equations (1) in $\Omega_l$, $\mathbf{w}_l$, $\mathbf{w}_{l-1}$, $\mathbf{w}|_{x=L}$ and $\mathbf{w}|_{x=0}$ denote $\mathbf{w}$ on $\Gamma_j$, $\Gamma_{j-1}$ and the lateral boundaries of $\Omega_l$ at $x = L$ and $x = 0$, respectively. In Section 5, we present an efficient method for approximating the operator $\Lambda$ by a matrix. If the electromagnetic field satisfies the quasi-periodic condition (17), we can eliminate the last two rows in (31) and find the reduced DtN map $\mathcal{M}$:

$$\mathcal{M} = \begin{bmatrix}\mathcal{M}_{11} & \mathcal{M}_{12}\\ \mathcal{M}_{21} & \mathcal{M}_{22}\end{bmatrix} = \begin{bmatrix}\Lambda_{11} & \Lambda_{12}\\ \Lambda_{21} & \Lambda_{22}\end{bmatrix} + \begin{bmatrix}\mathcal{C}_1\mathcal{D}_1 & \mathcal{C}_1\mathcal{D}_2\\ \mathcal{C}_2\mathcal{D}_1 & \mathcal{C}_2\mathcal{D}_2\end{bmatrix}, \tag{32}$$

where

$$\mathcal{C}_1 = \Lambda_{14} + \rho\Lambda_{13}, \quad \mathcal{C}_2 = \Lambda_{24} + \rho\Lambda_{23}, \quad \mathcal{D}_0 = \rho^2\Lambda_{43} - \rho\Lambda_{33} + \rho\Lambda_{44} - \Lambda_{34},$$
$$\mathcal{D}_1 = \mathcal{D}_0^{-1}(\Lambda_{31} - \rho\Lambda_{41}), \quad \mathcal{D}_2 = \mathcal{D}_0^{-1}(\Lambda_{32} - \rho\Lambda_{42}).$$

If $\Omega_l$ is a shifted unit cell containing two half air-holes, its DtN map is more difficult to calculate. Fortunately, all we need is the reduced DtN map $\mathcal{M}$ and it can be calculated from the reduced DtN map of a regular unit cell. In Fig. 3, we show the cross section of a shifted

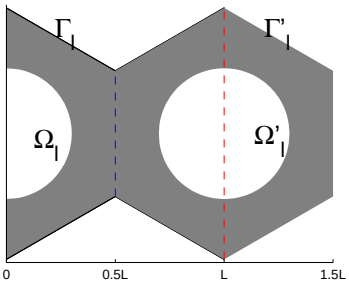


Fig. 3. A shifted unit cell $\Omega_l$ containing two half air-holes and the nearby regular unit cell $\tilde{\Omega}_l$.

unit cell $\Omega_l$ and its periodic extension in the $x$ direction by half a period. More precisely, we have a shifted unit cell for $0 < x < L$ and a regular unit cell $\Omega'_l$ for $L/2 < x < 3L/2$. For $\Omega'_l$, we can calculate its reduced DtN map $\mathcal{M}'$ by the method described earlier. To find the relation between $\mathcal{M}$ and $\mathcal{M}'$, we compare the boundaries $\Gamma_l$ and $\Gamma'_l$ of $\Omega_l$ and $\Omega'_l$, respectively. Notice that the second half of $\Gamma_l$ is identical to the first half of $\Gamma'_l$, the first half of $\Gamma_l$ is a horizontal translation of the second half of $\Gamma'_l$. The case for $\Gamma_{l-1}$ and $\Gamma'_{l-1}$ is similar. Therefore, if we order $\mathbf{w}_l$ and $\mathbf{w}_{l-1}$ as columns with two parts corresponding to $0 < x < L/2$ and $L/2 < x < L$, respectively, and order $\mathbf{w}'_l$ and $\mathbf{w}'_{l-1}$ (for $\mathbf{w}$ on $\Gamma'_l$ and $\Gamma'_{l-1}$) similarly, then

$$\mathbf{w}'_l = \mathcal{T}\mathbf{w}_l, \quad \mathbf{w}'_{l-1} = \mathcal{T}\mathbf{w}_{l-1} \quad \text{for} \quad \mathcal{T} = \begin{bmatrix} 0 & \mathcal{I} \\ \rho\mathcal{I} & 0 \end{bmatrix}, \tag{33}$$

where $\rho = e^{i\alpha_0 L}$ and $\mathcal{I}$ is an identity operator. This leads to

$$\mathcal{M} = \begin{bmatrix} \mathcal{T} & 0 \\ 0 & \mathcal{T} \end{bmatrix}^{-1} \mathcal{M}' \begin{bmatrix} \mathcal{T} & 0 \\ 0 & \mathcal{T} \end{bmatrix}. \tag{34}$$

## 4. Expansions in vertical modes

In actual numerical implementations, the operators $\mathcal{S}$, $\mathcal{Q}_l$, $\mathcal{Y}_l$, $\mathcal{M}$ and $\Lambda$, etc, have to be approximated by matrices. This is achieved by mode expansions in the vertical direction and discretization in physical space on the boundaries of the cross sections of the unit cells.

To account for out-of-plane radiations, we use the popular perfectly matched layer (PML) technique [23]. In terms of complex coordinate stretching [24], a PML replaces $z$ by $\hat{z} =$

$\int_0^z s(\tau)d\tau$ in the governing equation, where $s(z) \neq 1$ and is complex only if $z$ is in the PML. The variable $z$ is then truncated to the interval $(z_{bot}, z_{top})$, where the actual PMLs are given near the two ends of the interval. With the PMLs, the eigenvalue problem for the TE modes is modified as

$$\frac{\mu}{s}\frac{d}{dz}\left(\frac{1}{\mu s}\frac{d\phi^{(1)}}{dz}\right) + k_0^2\varepsilon\mu\phi^{(1)} = [\eta^{(1)}]^2\phi^{(1)}, \quad z_{bot} < z < z_{top}, \tag{35}$$

$$\phi^{(1)} = 0, \quad z = z_{top} \text{ and } z = z_{bot}, \tag{36}$$

and the eigenvalue problem for the TM modes is modified as

$$\frac{\varepsilon}{s}\frac{d}{dz}\left(\frac{1}{\varepsilon s}\frac{d\phi^{(2)}}{dz}\right) + k_0^2\varepsilon\mu\phi^{(2)} = [\eta^{(2)}]^2\phi^{(2)}, \quad z_{bot} < z < z_{top}, \tag{37}$$

$$\frac{d\phi^{(2)}}{dz} = 0, \quad z = z_{bot} \text{ and } z = z_{top}. \tag{38}$$

Notice that different boundary conditions are used for the TE and TM modes. Since $z$ is truncated to a finite interval, the above eigenvalue problems have discrete sequences of eigenvalues $\eta_j^{(p)}$ for $j = 1, 2, 3, ...$ and $p = 1, 2$. Therefore, PML gives a discrete approximation to the continuous spectra of open slab waveguides and allows us to write down the reflected and transmitted waves as in (8), (9), (10) and (11).

Let $\Sigma$ be a surface parallel to the $z$ axis and $\mathcal{A}$ be an operator that acts on the two $z$ components of the electromagnetic field, i.e., $\mathbf{w}$, where both $\mathbf{w}$ and $\mathcal{A}\mathbf{w}$ are defined on $\Sigma$, then we can get rid of the $z$ variable by expanding $\mu H_z$ and $\varepsilon E_z$, as well as the two components of $\mathcal{A}\mathbf{w}$ in the TE and TM modes, respectively. For the two $z$ components, we have

$$H_z(x, y, z) = \frac{1}{\mu(z)}\sum_{j=1}^{\infty}\tilde{H}_{z,j}(x, y)\,\phi_j^{(1)}(z), \quad E_z(x, y, z) = \frac{1}{\varepsilon(z)}\sum_{j=1}^{\infty}\tilde{E}_{z,j}(x, y)\,\phi_j^{(2)}(z). \tag{39}$$

Similarly, if $\mathcal{A}\mathbf{w} = [f, g]^T$, then on the surface $\Sigma$, we have

$$f(x, y, z) = \frac{1}{\mu(z)}\sum_{j=1}^{\infty}\tilde{f}_j(x, y)\,\phi_j^{(1)}(z), \quad g(x, y, z) = \frac{1}{\varepsilon(z)}\sum_{j=1}^{\infty}\tilde{g}_j(x, y)\,\phi_j^{(2)}(z). \tag{40}$$

In the above, $\tilde{H}_{z,j}$, $\tilde{E}_{z,j}$, $\tilde{f}_j$ and $\tilde{g}_j$ are functions defined on a curve $\Sigma^0$ which is the intersection of $\Sigma$ with the $xy$ plane. Clearly, the operator $\mathcal{A}$ can be represented by the following matrix $\tilde{\mathcal{A}}$ satisfying

$$\tilde{\mathcal{A}}\tilde{\mathbf{w}} = \begin{bmatrix}\tilde{\mathcal{A}}^{11} & \tilde{\mathcal{A}}^{12}\\ \tilde{\mathcal{A}}^{21} & \tilde{\mathcal{A}}^{22}\end{bmatrix}\tilde{\mathbf{w}} = \begin{bmatrix}\tilde{f}_1\\ \tilde{f}_2\\ \vdots\\ \tilde{g}_1\\ \tilde{g}_2\\ \vdots\end{bmatrix}, \quad \text{for} \quad \tilde{\mathbf{w}} = \begin{bmatrix}\tilde{H}_{z,1}\\ \tilde{H}_{z,2}\\ \vdots\\ \tilde{E}_{z,1}\\ \tilde{E}_{z,2}\\ \vdots\end{bmatrix}. \tag{41}$$

If we retain $J_1$ TE modes and $J_2$ TM modes, then $\tilde{\mathcal{A}}$ is a $J \times J$ matrix, where $J = J_1 + J_2$. At this stage, each entry of $\tilde{\mathcal{A}}$ is still an operator which acts on functions defined on the curve $\Sigma^0$. In the fully discretized case, each entry of $\tilde{\mathcal{A}}$ is approximated by a small matrix, the size of which corresponds to the number of points used to sample $\Sigma^0$. In the above, we have also written $\tilde{\mathcal{A}}$ in $2 \times 2$ block form. In that case, an entry of $\tilde{\mathcal{A}}$ may be written as $\tilde{A}^{pq}_{jk}$ for $1 \le p, q \le 2$, $j \ge 1$ and $k \ge 1$, and it is related to the two vertical modes $\phi^{(p)}_j$ and $\phi^{(q)}_k$.

With the vertical mode expansions, the operator $\mathcal{S}$ has a particular simple representation. In fact, $\tilde{\mathcal{S}}$ is diagonal. The diagonal entries $\tilde{\mathcal{S}}^{11}_{jj}$ and $\tilde{\mathcal{S}}^{22}_{jj}$ are linear operators defined on quasi-periodic functions of $x$, and they satisfy

$$\tilde{\mathcal{S}}^{pp}_{jj} \exp(i\alpha_k x) = \beta^{(p)}_{jk} \exp(i\alpha_k x), \quad k = 0, \pm 1, \pm 2, ... \tag{42}$$

for $p = 1$ and 2. If we discretize $x$ for $0 < x < L$ by $N$ uniform points, then $\tilde{\mathcal{S}}^{pp}_{jj}$ can be approximated by an $N \times N$ matrix whose eigenvalues are $\beta^{(p)}_{jk}$, the corresponding eigenvectors are the vectors obtained by evaluating $\exp(i\alpha_k x)$ at the $N$ points, and $k$ is given by $-N/2 \le k < N/2$ if $N$ is even and $|k| \le (N-1)/2$ if $N$ is odd.

The operators $\mathcal{Q}_l$, $\mathcal{Y}_l$, $\mathcal{M}$ and $\Lambda$ are represented in vertical mode expansions by $\tilde{\mathcal{Q}}_l$, $\tilde{\mathcal{Y}}_l$, $\tilde{\mathcal{M}}$ and $\tilde{\Lambda}$, respectively. Like the operator $\mathcal{A}$ discussed earlier, $\mathcal{Q}_l$ acts on $\mathbf{w}$ defined on $\Gamma_l$ and $\mathcal{Q}_l\mathbf{w}$ is also defined on $\Gamma_l$. However, the operator $\mathcal{Y}_l$ is slightly different, since it maps $\mathbf{w}$ on $\Gamma_l$ to $\mathbf{w}$ on $\Gamma_0$. Therefore, $\tilde{\mathcal{Y}}_l$ maps $\tilde{\mathbf{w}}$ on $\Gamma_l$ to $\tilde{\mathbf{w}}$ on $\Gamma_0$, and the entry $\tilde{\mathcal{Y}}_l|^{pq}_{jk}$ maps a function defined on $\Gamma^0_l$ to a function defined on $\Gamma^0_0$, where $\Gamma^0_l$ and $\Gamma^0_0$ are the intersections of $\Gamma_l$ and $\Gamma_0$ with the $xy$ plane. In particular, $\Gamma^0_0$ is simply the line segment given by $0 < x < L$, $y = 0$ and $z = 0$. If all operators are replaced by their representations in vertical mode expansions, and $\mathbf{w}$ is replaced by $\tilde{\mathbf{w}}$, then formulas and equations (24)-(32) remain valid.

## 5. Dirichlet-to-Neumann map of a unit cell

In this section, we present a method for constructing the DtN map of a regular unit cell $\Omega_l$ that contains a circular air-hole with radius $a$. The unit cell $\Omega_l$ is divided into the slab region and the hole region as shown in Fig. 4. We use a coordinate system, such that $z$-axis is the axis of the air-hole and the $xy$ plane is parallel to the slab. In the cylindrical coordinate system $\{r, \theta, z\}$, the slab and hole regions are given by $r > a$ and $r < a$, respectively. Similar to the construction of DtN maps for unit cells in ideal 2D PhCs [14, 15], we need to write down the general solution in the unit cell. The general solution can be obtained by using mode expansions in the vertical direction, cylindrical wave expansions in the horizontal plane and a proper matching on the vertical wall of the air-hole.

The general solution in the unit cell is first written as a Fourier series in $\theta$. For the two $z$

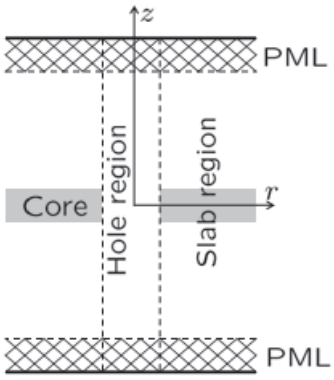


Fig. 4. Cross section of a regular unit cell $\Omega_l$ containing one air-hole. The vertical axis $z$ is terminated by PMLs.

components, we have

$$\mathbf{w}(r,\theta,z) = \sum_{m=-\infty}^{\infty} \hat{\mathbf{w}}_m(r,z)\, e^{im\theta}, \quad \text{where} \quad \hat{\mathbf{w}}_m(r,z) = \begin{bmatrix} \hat{H}_{z,m}(r,z) \\ \hat{E}_{z,m}(r,z) \end{bmatrix}. \tag{43}$$

In the slab region, the $m$-th Fourier mode can be expanded in vertical modes as

$$\hat{H}_{z,m} = \frac{1}{\mu(z)} \sum_{j=1}^{\infty} \left[ a_{jm}^{(1)} J_m(\eta_j^{(1)} r) + b_{jm}^{(1)} H_m^{(1)}(\eta_j^{(1)} r) \right] \phi_j^{(1)}(z), \quad r > a, \tag{44}$$

$$\hat{E}_{z,m} = \frac{1}{\varepsilon(z)} \sum_{j=1}^{\infty} \left[ a_{jm}^{(2)} J_m(\eta_j^{(2)} r) + b_{jm}^{(2)} H_m^{(1)}(\eta_j^{(2)} r) \right] \phi_j^{(2)}(z), \quad r > a, \tag{45}$$

where $J_m$ and $H_m^{(1)}$ are Bessel and Hankel functions, $\phi_j^{(p)}$ and $\eta_j^{(p)}$ are the mode profile and propagation constant of the $j$-th vertical TE ($p = 1$) or TM ($p = 2$) mode satisfying (35) and (36), or (37) and (38). For each $m$, the coefficients $b_{jm}^{(p)}$ (for all $j$) are related to $a_{jm}^{(p)}$. To find these relations, we need to write down the electromagnetic field in the hole region $r < a$. Let $\mu_h(z)$ and $\varepsilon_h(z)$ be the relative permeability and relative permittivity functions of the hole region, the vertical TE and TM modes in the hole region, denoted as $\phi_{h,j}^{(p)}$ and $\eta_{h,j}^{(p)}$, satisfy equations similarly to (35), (36), (37) and (38). Then, the $m$-th Fourier mode of $\mathbf{w}$ in the hole region is given by

$$\hat{H}_{z,m} = \frac{1}{\mu_h(z)} \sum_{j=1}^{\infty} c_{jm}^{(1)}\, J_m(\eta_{h,j}^{(1)}\, r)\, \phi_{h,j}^{(1)}(z), \quad r < a, \tag{46}$$

$$\hat{E}_{z,m} = \frac{1}{\varepsilon_h(z)} \sum_{j=1}^{\infty} c_{jm}^{(2)}\, J_m(\eta_{h,j}^{(2)}\, r)\, \phi_{h,j}^{(2)}(z), \quad r < a. \tag{47}$$

For each $m$, we define the vectors $\mathbf{a}_m$, $\mathbf{b}_m$ and $\mathbf{c}_m$ by

$$\mathbf{a}_m = \begin{bmatrix} a_{1m}^{(1)} \\ a_{2m}^{(1)} \\ \vdots \\ a_{1m}^{(2)} \\ a_{2m}^{(2)} \\ \vdots \end{bmatrix}, \quad \mathbf{b}_m = \begin{bmatrix} b_{1m}^{(1)} \\ b_{2m}^{(1)} \\ \vdots \\ b_{1m}^{(2)} \\ b_{2m}^{(2)} \\ \vdots \end{bmatrix}, \quad \mathbf{c}_m = \begin{bmatrix} c_{1m}^{(1)} \\ c_{2m}^{(1)} \\ \vdots \\ c_{1m}^{(2)} \\ c_{2m}^{(2)} \\ \vdots \end{bmatrix}, \tag{48}$$

then the continuity of $\hat{\mathbf{w}}_m$ at $r = a$ gives the following equation

$$B_{11}\mathbf{a}_m + B_{12}\mathbf{b}_m = B_{13}\mathbf{c}_m, \tag{49}$$

where the matrix $B_{11}$ and $B_{12}$ are obtained by evaluating (44) and (45) at $r = a^+$, and the matrix $B_{13}$ is obtained by evaluating (46) and (47) at $r = a^-$. In practice, the vertical mode expansions are truncated to keep $J_1$ TE modes and $J_2$ TM modes, then $\mathbf{a}_m$, $\mathbf{b}_m$ and $\mathbf{c}_m$ are vectors of length $J = J_1 + J_2$. We evaluate $\hat{H}_{z,m}$ and $\hat{E}_{z,m}$ at $J_1$ and $J_2$ distinct points of $z$, respectively, then $B_{11}$, $B_{12}$ and $B_{13}$ are $J \times J$ matrices.

Another equation for $\mathbf{a}_m$, $\mathbf{b}_m$ and $\mathbf{c}_m$ can be obtained by matching the $\theta$ components of the electromagnetic field at $r = a$. As before, we first expand the $\theta$ components of the electromagnetic field in Fourier series of $\theta$:

$$\begin{bmatrix} H_\theta \\ E_\theta \end{bmatrix} = \sum_{m=-\infty}^{\infty} \begin{bmatrix} \hat{H}_{\theta,m} \\ \hat{E}_{\theta,m} \end{bmatrix} e^{im\theta}. \tag{50}$$

In the slab region, we express the $m$-th Fourier mode in vertical mode expansions:

$$\begin{aligned}
\hat{H}_{\theta,m} &= \frac{im}{r\mu(z)} \sum_{j=1}^{\infty} \frac{\phi_j^{(1)\prime}(z)}{[\eta_j^{(1)}]^2} \left[ a_{jm}^{(1)} J_m(\eta_j^{(1)} r) + b_{jm}^{(1)} H_m^{(1)}(\eta_j^{(1)} r) \right] \\
&\quad + ik_0 \sum_{j=1}^{\infty} \frac{\phi_j^{(2)}(z)}{\eta_j^{(2)}} \left[ a_{jm}^{(2)} J_m'(\eta_j^{(2)} r) + b_{jm}^{(2)} H_m^{(1)\prime}(\eta_j^{(2)} r) \right], \quad r > a, \\
\hat{E}_{\theta,m} &= \frac{im}{r\varepsilon(z)} \sum_{j=1}^{\infty} \frac{\phi_j^{(2)\prime}(z)}{[\eta_j^{(2)}]^2} \left[ a_{jm}^{(2)} J_m(\eta_j^{(2)} r) + b_{jm}^{(2)} H_m^{(1)}(\eta_j^{(2)} r) \right] \\
&\quad - ik_0 \sum_{j=1}^{\infty} \frac{\phi_j^{(1)}(z)}{\eta_j^{(1)}} \left[ a_{jm}^{(1)} J_m'(\eta_j^{(1)} r) + b_{jm}^{(1)} H_m^{(1)\prime}(\eta_j^{(1)} r) \right], \quad r > a.
\end{aligned}$$

In the above, a prime is used to denote the derivative. Similarly, in the hole region, we have

$$\begin{aligned}
\hat{H}_{\theta,m} &= \sum_{j=1}^{\infty} \left[ \frac{imc_{jm}^{(1)}}{r\mu(z)} \frac{\phi_{h,j}^{(1)\prime}(z)}{[\eta_{h,j}^{(1)}]^2} J_m(\eta_{h,j}^{(1)} r) + \frac{ik_0 c_{jm}^{(2)}}{\eta_{h,j}^{(2)}} \phi_{h,j}^{(2)}(z) J_m'(\eta_{h,j}^{(2)} r) \right], \quad r < a, \\
\hat{E}_{\theta,m} &= \sum_{j=1}^{\infty} \left[ \frac{imc_{jm}^{(2)}}{r\varepsilon(z)} \frac{\phi_{h,j}^{(2)\prime}(z)}{[\eta_{h,j}^{(2)}]^2} J_m(\eta_{h,j}^{(2)} r) - \frac{ik_0 c_{jm}^{(1)}}{\eta_{h,j}^{(1)}} \phi_{h,j}^{(1)}(z) J_m'(\eta_{h,j}^{(1)} r) \right], \quad r < a.
\end{aligned}$$

The continuity of the $\theta$ components gives rise to the equation

$$B_{21}\mathbf{a}_m + B_{22}\mathbf{b}_m = B_{23}\mathbf{c}_m, \tag{51}$$

where $B_{21}$, $B_{22}$ and $B_{23}$ are $J \times J$ matrices, if $J_1$ TE modes and $J_2$ TM modes are retained in the above expansions, $\hat{H}_{\theta,m}$ and $\hat{E}_{\theta,m}$ are evaluated at $J_2$ and $J_1$ distinct points of $z$, respectively. From (49) and (51), we can eliminate $\mathbf{c}_m$ and solve $\mathbf{b}_m$ in terms of $\mathbf{a}_m$. Therefore, we can find a matrix $D_m$, such that

$$\mathbf{b}_m = D_m\, \mathbf{a}_m. \tag{52}$$

To find the DtN map $\Lambda$ of the unit cell $\Omega_l$, we use the general solution in the slab region given by (43), (44) and (45). Since we actually calculate the representation of $\Lambda$ in vertical mode expansions, i.e. $\tilde{\Lambda}$, it is more convenient to write the general solution by first expanding in the vertical modes. As in (39), we have

$$H_z = \frac{1}{\mu(z)} \sum_{j=1}^{\infty} \tilde{H}_{z,j}(r,\theta)\, \phi_j^{(1)}(z), \quad E_z = \frac{1}{\varepsilon(z)} \sum_{j=1}^{\infty} \tilde{E}_{z,j}(r,\theta)\, \phi_j^{(2)}(z) \tag{53}$$

where

$$\tilde{H}_{z,j}(r,\theta) = \sum_{m=-\infty}^{\infty} \left[ a_{jm}^{(1)} J_m(\eta_j^{(1)} r) + b_{jm}^{(2)} H_m^{(1)}(\eta_j^{(1)} r) \right] e^{im\theta}, \quad r > a, \tag{54}$$

$$\tilde{E}_{z,j}(r,\theta) = \sum_{m=-\infty}^{\infty} \left[ a_{jm}^{(2)} J_m(\eta_j^{(2)} r) + b_{jm}^{(2)} H_m^{(1)}(\eta_j^{(2)} r) \right] e^{im\theta}, \quad r > a. \tag{55}$$

Let $\Sigma$ be the lateral boundary of $\Omega_l$ and $\Sigma^0$ be the intersection of $\Sigma$ with the $xy$ plane. To obtain a matrix approximation of $\tilde{\Lambda}$, we choose $K$ points on $\Sigma^0$, say $\mathbf{x}_1$, $\mathbf{x}_2$, ..., $\mathbf{x}_K$, retain $K$ terms for the sums in (54) and (55), and evaluate $\tilde{H}_{z,j}$ and $\tilde{E}_{z,j}$ at these $K$ points for $1 \le j \le J_1$ and $1 \le j \le J_2$, respectively. This gives rise to

$$\tilde{\mathbf{w}} = F\mathbf{a}, \tag{56}$$

where $\tilde{\mathbf{w}}$, as given in (41), is a column vector for all $\tilde{H}_{z,j}$ and $\tilde{E}_{z,j}$, $\mathbf{a}$ is a column vector for all $a_{jm}^{(p)}$ and $F$ is a square matrix. Notice that $\tilde{H}_{z,j}$ and $\tilde{E}_{z,j}$ are themselves column vectors of length $K$, thus the total length of $\tilde{\mathbf{w}}$ is $JK$ for $J = J_1 + J_2$. The sums in (54) and (55) are truncated to $-K/2 \le m < K/2$ for an even $K$ or to $|m| < (K-1)/2$ for an odd $K$. Since for each $m$, the vector $\mathbf{a}_m$ has length $J$, the total length of $\mathbf{a}$ is thus $JK$. The general solution given in (54) and (55) involves the coefficients $b_{jm}^{(p)}$. However, since $b_{jm}^{(p)}$ (for $p = 1$, 2, and $j \ge 1$) are related to $a_{jm}^{(p)}$ as given in (52), $\tilde{\mathbf{w}}$ is only related to $\mathbf{a}$.

At the $K$ points on $\Sigma^0$, we also specify a unit normal vector $\nu(\mathbf{x}_k)$ for $k = 1, 2, ..., K$. Since the general solution is given analytically in (54) and (55), we can easily evaluate the directional derivatives of $\tilde{H}_{z,j}$ and $\tilde{E}_{z,j}$ at these $K$ points. This leads to

$$\frac{\partial \tilde{\mathbf{w}}}{\partial \nu} = G\mathbf{a}, \tag{57}$$

where $G$ is a $(JK) \times (JK)$ square matrix. Eliminating the coefficients $\mathbf{a}$ from (56) and (57), we obtain the matrix approximation $\tilde{\Lambda}$ of the DtN map satisfying

$$\frac{\partial \tilde{\mathbf{w}}}{\partial \nu} = \tilde{\Lambda}\tilde{\mathbf{w}}, \quad \tilde{\Lambda} = GF^{-1}. \tag{58}$$

## 6. Computing the vertical modes

To implement the method presented in previous sections, we need to calculate the vertical TE and TM modes for both slab and hole regions, assuming that the $z$ axis is truncated by PMLs. In the slab region, the vertical modes are solutions of the eigenvalue problems (35) and (36), or (37) and (38) for the TE and TM cases, respectively. In the hole region, the governing equations can be simply obtained by replacing $\mu(z)$ and $\varepsilon(z)$ in (35) and (37) by $\mu_h(z)$ and $\varepsilon_h(z)$. For a layered structure where $\mu$ and $\varepsilon$ are piecewise constant in $z$, the eigenvalue problems can be solved semi-analytically by writing down the exact solution of $\phi^{(p)}$ in terms of $[\eta^{(p)}]^2$ and solving an equation for $[\eta^{(p)}]^2$. This approach is not as convenient as it appears, since many modes are needed in the vertical mode expansions and $[\eta^{(p)}]^2$ is usually complex due to the use of PMLs. It is difficult to find all complex solutions of $[\eta^{(p)}]^2$ in a given region of the complex plane. Furthermore, the eigenvalue problems give infinite sequences of TE and TM modes, but it is not clear how the sequences should be truncated, since there is no natural ordering for the complex eigenvalues $[\eta^{(p)}]^2$. Some of these difficulties can be avoided by solving the eigenvalue problems numerically. For improved accuracy and to reduce the total number of vertical modes, a high order numerical scheme is preferred.

For the governing equations (35) and (37), a fourth order finite difference scheme was previously developed by Chiou *et al.* [33]. If $\phi$ is a sufficiently smooth function of $z$, we have the following well-known fourth order compact finite difference scheme:

$$\frac{\phi(z-h) - 2\phi(z) + \phi(z+h)}{h^2} = \frac{\phi''(z-h) + 10\phi''(z) + \phi''(z+h)}{12} + O(h^4), \tag{59}$$

where $\phi''$ is the second derivative of $\phi$ and $h$ is the grid size. Chiou *et al.* derived a similar formula for the case where the interval $[z-h, z+h]$ contains a discontinuity of $\mu(z)$ or $\varepsilon(z)$ and applied the formula to (35) and (37).

In our problem, the $z$-derivatives of the vertical modes are also needed. In the construction of the DtN map of a unit cell, we match the $\theta$ components of the electromagnetic field on

the vertical boundary of the hole. It turns out that $H_\theta$ involves the TM modes and the $z$-derivatives of the TE modes, and $E_\theta$ involves the TE modes and the $z$-derivative of the TM modes. Therefore, it is more convenient to rewrite (35) and (37) as first order systems and approximate the first order derivative operator. For this purpose, we also use staggered grids, so that the TE modes and the $z$-derivatives of the TM modes are discretized at the integer grid points $\{z_l : l = 1, 2, ...\}$, and the TM modes and the $z$-derivatives of the TE modes are discretized at the half-integer grid points $\{z_{l+\frac{1}{2}} : l = 0, 1, ...\}$, where $z_{l+\frac{1}{2}} = z_l + h/2$. If $f$ is a smooth function of $z$, we have the following fourth order finite difference schemes:

$$\frac{f(z+h/2) - f(z-h/2)}{h} = \frac{f'(z-h) + 22f'(z) + f'(z+h)}{24} + O(h^4). \tag{60}$$

We need an extension of (60) to cases where $f$ or its derivatives have a discontinuity at $z_* \in [z-h, z+h]$. We write the extended formula as

$$d_1 f(z+h/2) + d_2 f(z-h/2) \approx d_3 f'(z-h) + d_4 f'(z) + d_5 f'(z+h), \tag{61}$$

where the coefficients $d_1$, $d_2$, ..., $d_5$ depend on $h$, the location of $z_*$ and the exact matching conditions at $z_*$, and they satisfy $d_3 + d_4 + d_5 = 1$. If $z_*$ coincides with one of five involved points: $z$, $z \pm h/2$ and $z \pm h$, and if $f$ and $f'$ are not continuous at $z_*$, then $f(z_*)$ and $f'(z_*)$ in (61) should be replaced by their one-sided limits $f(z_*^-)$ and $f'(z_*^-)$.

To discretize (35) and (37), the formula (61) is needed for the following four cases: (1) $f = \phi^{(1)}$ and $z = z_{l+\frac{1}{2}}$, (2) $f = d\phi^{(1)}/dz$ and $z = z_l$, (3) $f = \phi^{(2)}$ and $z = z_l$, and (4) $f = d\phi^{(2)}/dz$ and $z = z_{l+\frac{1}{2}}$. For each of these four cases, the coefficients $d_1$, $d_2$, ..., $d_5$ are derived following the procedure developed in [33]. It relies on Taylor expansions and the exact matching conditions at $z_*$ for $\phi^{(p)}$ and its derivatives. Assuming $\mu(z)$ or $\varepsilon(z)$ are piecewise constant and discontinuous at $z_*$, then the basic matching conditions are

$$\begin{aligned}
\phi^{(p)}(z_*^-) &= \phi^{(p)}(z_*^+), \quad p = 1, 2, \\
\frac{1}{\mu(z_*^-)} \frac{d\phi^{(1)}}{dz}(z_*^-) &= \frac{1}{\mu(z_*^+)} \frac{d\phi^{(1)}}{dz}(z_*^+), \\
\frac{1}{\varepsilon(z_*^-)} \frac{d\phi^{(2)}}{dz}(z_*^-) &= \frac{1}{\varepsilon(z_*^+)} \frac{d\phi^{(2)}}{dz}(z_*^+).
\end{aligned}$$

The matching conditions for higher order derivatives of $\phi^{(p)}$ are also needed in the derivation of (61) and they can obtained from the differential equations (35) and (37).

In the PMLs, $\mu(z)$ and $\varepsilon(z)$ are supposed to be constants, then (35) and (37) are reduced to

$$\frac{d^2\phi^{(p)}}{d\hat{z}^2} + k_0^2 \varepsilon\mu\, \phi^{(p)} = [\eta^{(p)}]^2 \phi^{(p)}, \tag{62}$$

where $\hat{z} = \int_0^z s(\tau) d\tau$ is a complex function of $z$. Corresponding to the real grid points $z_l$ and $z_{l+\frac{1}{2}}$ with a constant grid size $h$, we have the complex grid points $\hat{z}_l$ and $\hat{z}_{l+\frac{1}{2}}$. To discretize

(62), we need to extend the formula (60) to non-uniform grids, then apply the extended formula to the complex grid points of $\hat{z}$.

In our implementation, the interval $(z_{bot}, z_{top})$ is discretized as

$$\begin{aligned} z_l &= z_{bot} + lh, \quad 1 \le l \le J_1 \\ z_{l+\frac{1}{2}} &= z_{bot} + (l + \frac{1}{2})h, \quad 0 \le l \le J_1, \end{aligned}$$

where $h = (z_{top} - z_{bot})/(J_1 + 1)$. Therefore, a TE mode $\phi^{(1)}$ is represented by a vector of length $J_1$ and a TM mode $\phi^{(2)}$ is represented by a vector of length $J_2 = J_1 + 1$. This difference in the length of the vectors reflects the different boundary conditions used for the TE and TM modes. We have also chosen the truncation and discretization parameters $z_{bot}$, $z_{top}$ and $J_1$, such that the material interfaces (discontinuities of $\varepsilon$ and/or $\mu$) are located at integer grid points. In that case, it can be shown that formula (61) retains a fourth order accuracy.

## 7. Numerical examples

To demonstrate our method, we calculate the transmission and reflection spectra for a number of examples. The first example was previously analyzed by Ochiai and Sakoda [34] using the FDTD method. The structure involves $l_* = 10$ arrays of air-holes on a slab with a dielectric constant $\varepsilon = 11.56$. The slab is surrounded by air. The air-holes form a triangular lattice with lattice constant $L$. The radius of the air-holes and thickness of the slab are $0.25L$ and $0.5L$, respectively. For a normal incident wave which is the fundamental TE mode of the slab, we obtain the transmission spectrum shown in Fig. 5(top), where the vertical axis is the transmittance defined in Section 2 and the horizontal axis is the normalized frequency. In agreement with the results given in [34], there is a frequency interval (which contains a bandgap) where the transmission is very low. However, outside that interval, the transmittance we obtained is somewhat larger than that given in [34]. In Fig. 5(bottom), we show the out-of-plane radiation loss for different frequencies. Although this loss is relatively small (less than 5%) for small frequencies ($\omega L/(2\pi c) < 0.32$), it can be more than 25% for some larger frequencies satisfying $\omega L/(2\pi c) > 0.36$.

To obtain the results shown in Fig. 5, we truncate the $z$ variable to the interval $(-3L, 3L)$ with PMLs given by $2.5L < |z| < 3L$, and discretize $z$ using the grid size $h = L/8$. The parameters of PMLs are chosen based on the principles developed in [35]. Since a fourth order scheme is used to discretize vertical variable $z$, the grid size $h$ is relatively large. This leads to $J_1 = 47$ TE modes, $J_2 = 48$ TM modes and a total of $J = 95$ modes. For a hexagon unit cell, we use 7 points to discretize each edge of $\Sigma^0$ (boundary of the intersection of the hexagon unit cell with the $xy$ plane), thus the total number of points to discretize $\Sigma^0$ is $K = 42$. As a result, the DtN map $\Lambda$ is approximated by a $3990 \times 3990$ matrix, and the operators $\mathcal{Q}_l$ and $\mathcal{Y}_l$ $(0 < l < l_*)$ are approximated by $1330 \times 1330$ matrices. The line segments $\Gamma_0^0$ and

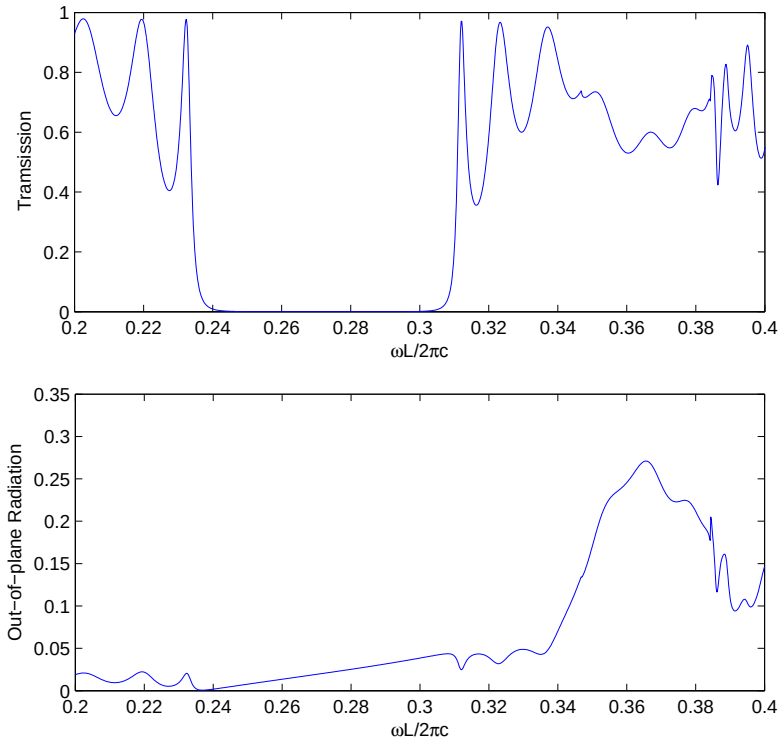


Fig. 5. Transmission spectrum and out-of-plane radiation loss of 10 arrays of air-holes on a slab for a fundamental TE mode incident wave at normal incidence.

$\Gamma^0_{l_*}$ (for $0 < x < L$ and $y = 0$, $y = D$) are discretized by $N = 12$ points. Therefore, $\mathcal{Q}_0$, $\mathcal{Y}_0$, $\mathcal{Q}_{l_*}$, $\mathcal{Y}_{l_*}$ and $\mathcal{S}$ are approximated by $1140 \times 1140$ matrices. The most expensive step of our method is to calculate the DtN map of the unit cells. It requires solving linear systems with a $3990 \times 3990$ coefficient matrix.

The second example is also a slab with a triangular lattice of air-holes and surrounded by air, but the parameters are different. We assume that the dielectric constant of the slab is $\varepsilon = 12.25$, the thickness of the slab is $0.6L$, and the radius of the air-holes is $0.3L$. The band structure of such a PhC slab has been calculated by a plane-wave expansion method in [36]. In the first case, we calculate the transmission and reflection spectra and out-of-plane radiation loss for finite number of air-hole arrays, where the incident wave is the fundamental TE mode propagating towards the arrays with an angle of incidence $\theta^{(1)}_{1,0} = \pi/6$. The transmission spectrum for $l_* = 7$ arrays is shown in Fig. 6. For this case, the out-of-plane radiation loss is bounded by 2% for all frequencies given in Fig. 6 and it is very small for $\omega L/(2\pi c) \leq 0.32$. For this example, we consider another case where the air-hole arrays are separated by a line defect as shown in Fig. 7. The structure can be obtained by filling the air-holes of the central

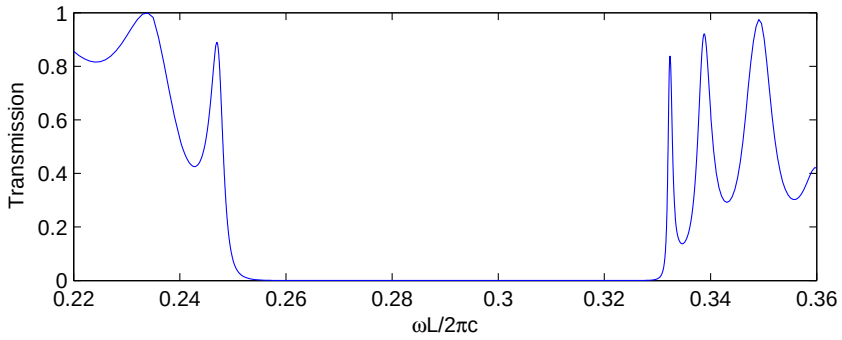


Fig. 6. Transmission spectrum of 7 arrays of air-holes for a fundamental TE mode incident wave with an incident angle $\pi/6$.

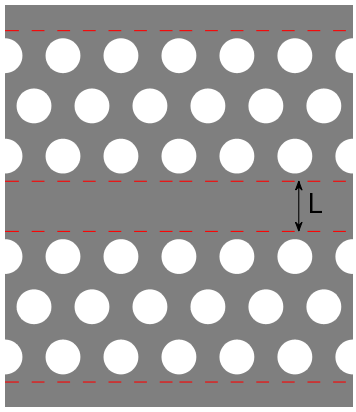


Fig. 7. Top view of 6 arrays of air-holes on a slab separated by a line defect.

array, and it corresponds to a leaky waveguide with finite PhC cladding in the horizontal plane. Although there are only six air-hole arrays, we still use $l_* = 7$ unit cells in our operator marching scheme, since a defect unit cell without an air-hole is needed. For this structure, we calculate the transmission and reflection spectra for the same incident wave. The results are shown in Fig. 8. Clearly, there are a few resonant transmission frequencies in the originally low transmission frequency interval. To reveal more details, we show the transmission spectra near the resonant frequencies with a very dense sampling of the frequency. It appears that the transmission peaks at the resonant frequencies are correctly calculated. For this case, the out-of-plane radiation loss remains small for non-resonant frequencies, but it is much larger at the resonant frequencies. The largest out-of-plane loss is about 25% and it corresponds to the resonant frequency near $\omega L/(2\pi c) = 0.31$.

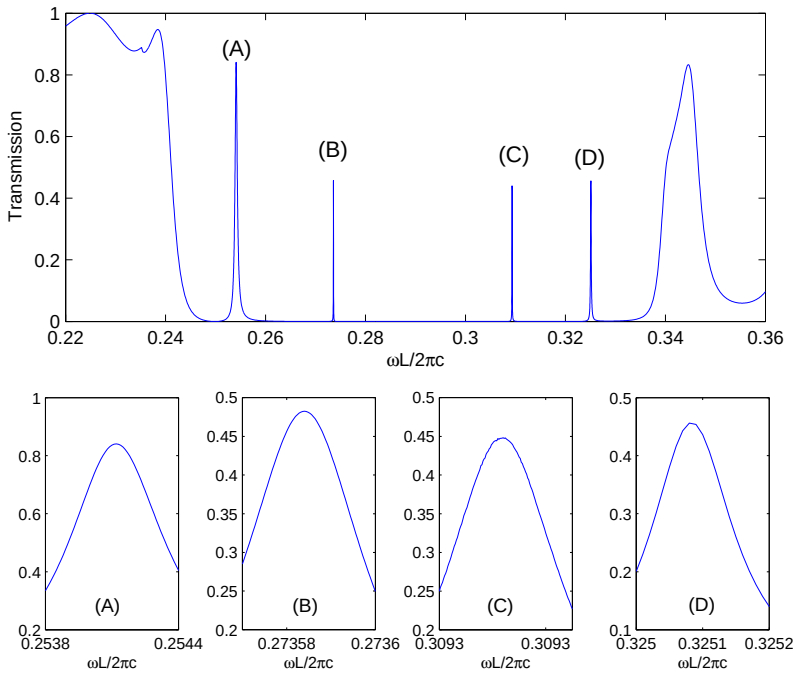


Fig. 8. Transmission spectrum of 6 arrays of air-holes on a slab separated by a line defect for a fundamental TE mode incident wave with incident angle $\pi/6$.

The numerical results shown in Fig. 6 and Fig. 8 are obtained by truncating $z$ to the interval $(-3.3L, 3.3L)$, discretizing $z$ by the grid size $h = 0.15L$, discretizing each edge of $\Sigma^0$ by 7 points and discretizing the line segments $\Gamma_0^0$ and $\Gamma_{l_*}^0$ by $N = 12$ points. Therefore, the total number of vertical modes is $J = 87$, $\tilde{\Lambda}$ is a $3654 \times 3654$ matrix, $\tilde{\mathcal{Q}}_l$ and $\tilde{\mathcal{Y}}_l$ $(0 < l < l_*)$ are $1218 \times 1218$ matrices, $\tilde{\mathcal{Q}}_0$, $\tilde{\mathcal{Y}}_0$, $\tilde{\mathcal{Q}}_{l_*}$, $\tilde{\mathcal{Y}}_{l_*}$ and $\tilde{\mathcal{S}}$ are $1044 \times 1044$ matrices.

## 8. Conclusions

In this paper, we developed a rigorous and efficient method to compute transmission and reflection spectra for finite number of air-hole arrays in a slab, where the incident waves are propagating modes of the slab. The study is relevant to photonic crystal slabs which have promising applications in future photonic integrated circuits. Our method is a 3D extension of an earlier Dirichlet-to-Neumann (DtN) map method [15–17] for ideal 2D photonic crystals which are invariant in one spatial direction. It is a rigorous computational method without any analytic approximations. The method relies on the DtN maps of the unit cells defined in terms of the two $z$ components of the electromagnetic field, where the vertical $z$ direction is perpendicular to the horizontal plane of the slab. The DtN maps are constructed based on mode expansions in the vertical direction and cylindrical wave expansions in the horizontal

plane.

Compared with the widely used FDTD and finite element methods, our method has the advantage of avoiding a full discretization of a 3D volume. In particular, repeated calculations in identical unit cells are avoided. The multipole method [11] also uses vertical mode and cylindrical wave expansions, but it requires sophisticated lattice sums techniques to account for the infinite number of cylinders in each array. The DtN avoids lattice sums and is relatively simple to implement.

## Acknowledgments

This research was partially supported by a grant from City University of Hong Kong (Project No. 7008054).

## References

1. J. D. Joannopoulos, S. G. Johnson, J. N. Winn, and R. D. Meade, Photonic Crystals: Molding the Flow of Light, 2nd Ed., (Princeton University Press, Princeton, NJ, 2008).
2. M. Qiu, "Effective index method for heterostructure-slab-waveguide based two-dimensional photonic crystals," Appl. Phys. Lett. **8**, 1163-1165 (2002).
3. C. Ciminelli, F. Peluso, and M. N. Armenise, "Modeling and design of two-dimensional guided-wave photonic band-gap devices," J. Lightwave Technol. **23**, 886-901 (2005).
4. A. Taflove and S. C. Hagness, *Computational Electrodynamics: the finite-difference time-domain method*, 2nd ed., (Artech House, 2000).
5. G. Bao Z. M. Chen and H. J. Wu, "Adaptive finite-element method for diffraction gratings", J. Opt. Soc. Am. A **22**, 1106-1114 (2005).
6. Y. J. Li and J. M. Jin, "Fast full-wave analysis of large-scale three-dimensional photonic crystal devices," J. Opt. Soc. Am. B **24**, 2406-2415 (2007).
7. P. A. Martin, Multiple Scattering: Interaction of Time-Harmonic Waves with $N$ Obstacles, Cambridge University Press, 2006.
8. E. Centeno, D. Felbacq, "Rigorous vector diffraction of electromagnetic waves by bidimensional photonic crystals," J. Opt. Soc. Am. A **17**, 320-327 (2000).
9. G. H. Smith, L. C. Botten, R. C. McPhedran, and N. A. Nicorovici, "Cylinder gratings in conical incidence with applications to woodpile structures," Phys. Rev. E **67**, 056620 (2003).
10. K. Yasumoto, H. Toyama and T. Kushta, "Accurate analysis of two-dimensional electromagnetic scattering from multilayered periodic arrays of circular cylinders using lattice sums technique," IEEE Transactions on Antennas and Propagation **52**, 2603-2611 (2004).
11. S. Boscolo and M. Midrio, "Three-dimensional multiple-scattering technique for the analysis of photonic-crystal slabs," J. Lightwave Technol. **22**, 2778-2786 (2004).

12. S. Venakides, M. A. Haider, and V. Papanicolaou, "Boundary integral calculations of two-dimensional electromagnetic scattering by photonic crystal Fabry-Perot structures," SIAM Journal on Applied Mathematics **60**, 1686-1706 (2000).
13. D. Pissoort, E. Michielssen, D. V. Ginste, and F. Olyslager, "Fast-multipole analysis of electromagnetic scattering by photonic crystal slabs," J. Lightwave Technol. **25**, 2847-2863 (2007).
14. J. Yuan and Y. Y. Lu, "Photonic bandgap calculations using Dirichlet-to-Neumann maps," J. Opt. Soc. Am. A **23**, 3217-3222 (2006).
15. Y. Huang and Y. Y. Lu, "Scattering from periodic arrays of cylinders by Dirichlet-to-Neumann maps," J. Lightwave Technol. **24**, 3448-3453 (2006).
16. Y. Huang and Y. Y. Lu, "Modeling photonic crystals with complex unit cells by Dirichlet-to-Neumann maps," Journal of Computational Mathematics, **25**, 337-349 (2007).
17. Y. Wu and Y. Y. Lu, "Dirichlet-to-Neumann map method for analyzing interpenetrating cylinder arrays in a triangular lattice," J. Opt. Soc. Am. B **25**, 1466-1473 (2008).
18. Y. Wu and Y. Y. Lu, "Dirichlet-to-Neumann map method for analyzing periodic arrays of cylinders with oblique incident waves," J. Opt. Soc. Am. B **26**, 1442-1449 (2009).
19. Y. Wu and Y. Y. Lu, "Dirichlet-to-Neumann map method for analyzing crossed arrays of circular cylinders," J. Opt. Soc. Am. B **26**, 1984-1993 (2009).
20. Z. Hu and Y. Y. Lu, "Efficient analysis of photonic crystal devices by Dirichlet-to-Neumann maps," Opt. Express **16**, 17383-17399 (2008).
21. Z. Hu and Y. Y. Lu, "Improved Dirichlet-to-Neumann map method for modeling extended photonic crystal devices," Opt. Quant. Electron. **40**, 921-932 (2008).
22. C. Vassallo, Optical Waveguide Concepts, Elsevier, Amsterdam, 1991.
23. J. P. Berenger, "A perfectly matched layer for the absorption of electromagnetic waves," J. Comput. Phys. **114**, 185-200 (1994).
24. W. C. Chew and W. H. Weedon, "A 3D perfectly matched medium from modified Maxwells equations with stretched coordinates," Microwave and Optical Technology Letters **7**, 599-604 (1994).
25. M. G. Moharam, D. A. Pommet, E. B. Grann, and T. K. Gaylord, "Stable implementation of the rigorous coupled-wave analysis for surface-relief gratings – enhanced transmittance matrix approach," J. Opt. Soc. Am. A **12**, 1077-1086 (1995).
26. N. P. K. Cotter, T. W. Preist and J. R. Sambles, "Scattering-matrix approach to multilayer diffraction," J. Opt. Soc. Am. A **12**, 1097-1103 (1995).
27. L. Li, "Formulation and comparison of two recursive matrix algorithms for modeling layered diffraction gratings," J. Opt. Soc. Am. A **13**, 1024-1035 (1996).
28. P. Lalanne, "Electromagnetic analysis of photonic crystal waveguides operating above the light cone," IEEE Journal of Quantum Electronics **38**, 800-804 (2002).

29. M. Dems, R. Kotynski and K. Panajotov, "Plane wave admittance method – a novel approach for determining the electromagnetic modes in photonic structures," Opt. Express **13**, 3196-3207 (2005).
30. Y. Y. Lu and J. R. McLaughlin, "The Riccati method for the Helmholtz equation," Journal of the Acoustical Society of America **100**, 1432-1446 (1996).
31. Y. Y. Lu, "Some techniques for computing wave propagation in optical waveguides," Communications in Computational Physics **1**, 1056-1075 (2006).
32. L. Yuan and Y. Y. Lu, "An efficient bidirectional propagation method based on Dirichlet-to-Neumann maps," IEEE Photon. Technol. Lett. **18**, 1967-1969 (2006).
33. Y. P. Chiou, Y. C. Chiang, and H. C. Chang, "Improved three-point formulas considering the interface conditions in the finite-difference analysis of step-index optical devices," J. Lightwave Technol. **18**, 243-251 (2000).
34. T. Ochiai and K. Sakoda, "Dispersion relation and optical tranmittance of a hexagon photonic crystal slab," Phys. Rev. B **63**, 125107 (2001).
35. Y. Y. Lu, "Minimizing the discrete reflectivity of perfectly matched layers," IEEE Photon. Technol. Lett. **18**, 487-489 (2006).
36. S. Shi, C. Chen, and D. W. Prather, "Plane-wave expansion method for calculating band structure of photonic crystal slabs with perfectly matched layers," J. Opt. Soc. Am. A **21**, 1769-1775 (2004).